Biomed Microdevices (2014) 16:439–447
DOI 10.1007/s10544-014-9846-4

Well-plate mechanical confinement platform for studies of mechanical mutagenesis

H. Kittur · W. Weaver · D. Di Carlo

Published online: 13 March 2014

Abstract Limited space for cell division, perhaps similar to the compressed microenvironment of a growing tumor, has been shown to induce phenotypic and karyotypic changes to a cell during mitosis. To expand understanding of this missegregation of chromosomes in aberrant multi-daughter or asymmetric cell divisions, we present a simple technique for subjecting mammalian cells to adjustable levels of confinement which allows subsequent interrogation of intracellular molecular components using high resolution confocal imaging. PDMS micropatterned confinement structures of subcellular height with neighboring taller media reservoir channels were secured on top of confluent cells with a custom compression well-plate system. The system improved ease of use over previous devices since confined cells could be initially grown on glass coverslips in a 12-well plate, and subsequently be imaged by high resolution confocal imaging, or during compression by live cell imaging. Live cell imaging showed a significant increase in abnormal divisions of confined cells across three different cell lines (HeLa, A375, and A549). Immunofluoresecence stains revealed a significant increase in cell diameter and chromosome area of confined cells, but no significant increase in centrosome-centromere distance upon division when compared to unconfined cells. The developed system could open up studies more broadly on confinement effects on mitotic processes, and increase the throughput of such studies.

Keywords Confinement · Mitosis · Cytokinesis · Multipolar · Asymmetric · Aneuploidy

1 Introduction

Chromosomal instability (CIN), characterized by rapid variations in chromosome number, is largely the result of chromosomal missegregation during mitosis. Inevitably, this leads to aneuploidy, a significant hallmark of cancer (Gordon et al. 2012). This phenomenon has been induced experimentally and studied extensively through numerous avenues, including centrosome amplification (Borel et al. 2002; Ganem et al. 2009; Lingle et al. 2002; Pihan et al. 2003), radiation (Limoli et al. 2001), and DNA hypomethylation (Menendez et al. 2004; Nishigaki et al. 2005; Wilson et al. 2007). Yet, despite such studies, the mechanisms leading to the development of CIN *in vivo* have not been fully identified.

Recently, the influence of force balance on the proper segregation of chromosomes has been a subject of study. Under normal conditions, as cells enter M phase, the nuclear envelope and interphase microtubules (MT) disintegrate. Kinetochore microtubules (k-MT) extend from the centrosomes via various Ran GTPase-activated MT-associated proteins (MAPs) (Hetzer et al. 2002) and attach to the chromosome kinetochores through precise control of Aurora-B-kinase-dependent phosphorylation of Hec1 (DeLuca et al. 2011), and regulation of small Rho GTPases such as Cdc42 (Yasuda et al. 2004). This is coupled with increased hydrostatic pressure (Stewart et al. 2011) to drive cell rounding, as well as cortical cues, including force (Tseng et al. 2012), that regulate local astral MT stability (Théry et al. 2005) which assist in

Electronic supplementary material The online version of this article (doi:10.1007/s10544-014-9846-4) contains supplementary material, which is available to authorized users.

H. Kittur · W. Weaver · D. Di Carlo (✉)
University of California – Los Angeles, Los Angeles, CA, USA
e-mail: dicarlo@seas.ucla.edu

D. Di Carlo
California NanoSystems Institute, Los Angeles, CA, USA

D. Di Carlo
Jonsson Comprehensive Cancer Center, Los Angeles, CA, USA

positioning the centrosomes at opposite poles. The establishment of this bipolar spindle is followed by an alignment of the chromosomes at the spindle midzone, forming a metaphase plate (Ditchfield et al. 2003). The spindle assembly checkpoint (SAC), a complex, highly sensitive ensemble of proteins ensures that all of these steps have occurred properly before allowing progression into anaphase, where the spindle fibers draw the sister chromatids to opposite poles.

Yet, external forces that can originate from the tumor microenvironment can disrupt these intricate mitotic processes. Previous studies have shown that cells that are uniaxially confined with stiff (~1 MPa) substrates display startlingly high frequencies of delayed mitosis, cell death, asymmetric division, cell fusion, and multi-polar cytokinesis (Tse et al. 2012), as illustrated in Fig. 1. The absence of sufficient space to establish proper cell rounding results in mitotic delays (Tse et al. 2012); displacement of the chromosomes from proper metaphase alignment activates spindle assembly checkpoint proteins Bub1 and Mad1 to impede mitotic progression until alignment is signaled to be sufficient (Itabashi et al. 2012; Lancaster et al. 2013). Prolonged exposure to such conditions appears to result in a decision at the cellular level down one of two routes: the cell may initiate apoptosis, or it may proceed through the checkpoint and attempt cytokinesis. The latter may occur, despite failure of the k-MTs to gather all of the chromosomes to the metaphase plate, resulting in chromosome mis-segregation (Lancaster et al. 2013).

Depending on the location of formation of the spindle apparatus, the cell may initiate an uneven separation of its cytosol, producing daughters of significantly different sizes. In cells that contain additional centrosomes, which also establish poles by extending k-MTs to segregate chromosomes, more than two progeny can result – a process which is reduced in normal divisions where centrosomes can cluster at two poles symmetrically around a well-defined plane (Borel et al. 2002; Ganem et al. 2009; Krämer et al. 2011). From any of these aberrations, the daughters are highly likely to carry aneuploid karyotypes. Yet another pathway exists, in which several or all of the daughter cells re-fuse, which may also produce aneuploid cells (Lu and Kang 2009). Severe aneuploidy may trigger apoptosis, but should the cells remain viable, they will carry their abnormal genetic material to the next cell cycle, which could lead to CIN and accelerate tumorigenesis.

The intracellular mechanisms of confined HeLa cells have been studied extensively by Lancaster et al. (2013). Yet, many questions remain concerning mitotic processes during confinement, particularly the genes and protein localization that influence decisions such as: How is the metaphase plate assembled in such conditions? What influences the decision to proceed with an abnormal cytokinesis? What molecular or physical cues are at the top of the hierarchy of the assembly of the mitotic spindle apparatus? Additionally, confinement studies may shed more light into the fate of supernumerary centrosomes and the mechanisms behind formation of cleavage furrows in cells of flattened geometries. Finally, a solid connection to *in vivo* occurrences of confined cells of various tissue origins has yet to be established. Insights in how mitotic processes function in these perturbed conditions also enables a better understanding of the machinery of normal mitotic processes and the strategies the cell uses to ensure the robustness of this process.

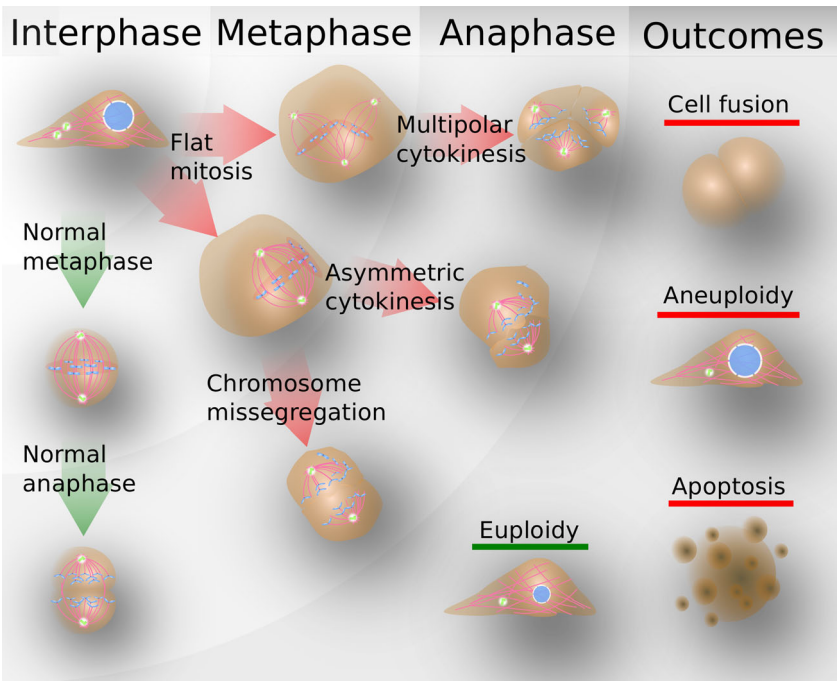

Fig. 1 Mitotic progression of mechanically stressed cells. Flat divisions increase the frequency of chromosome missegregation, which can lead to asymmetric daughters and more than two daughter cells. If the cell remains viable, it is likely to be aneuploid, but in some cases daughters may fuse with each other or with neighboring cells

To better understand the fundamental intracellular mechanisms behind the impact of physical constraint on cell growth and division, we have developed an inexpensive and easy-to-use tool for confining a massive array of cells to predetermined heights. It offers a unique advantage over other designs (Le Berre et al. 2012; Tse et al. 2012) in its simplicity and its ability to permit solution exchange. We describe methods of implementing this device for long-term live video capture, as well as for fluorescence staining and high resolution confocal imaging. As proof-of-concept, we applied the technology to perform confined culture of three cancer cell lines—HeLa, A549, and A375—which are of varying origin, morphology, and genotype, and therefore display unique responses to confinement. HeLa cells are described as hypertriploid ($3N^{+}$), with 22–25 abnormal chromosomes out of a total of 76–80 chromosomes (Macville et al. 1999). On the other hand, A375 and A549 cells are hypotriploid ($3N^{-}$), each with 60–63 chromosomes (Luk et al. 2001). Furthermore, each of these cell lines is characterized by a unique set of losses and gains in chromosomes and chromosome regions.

2 Device properties

We have developed a versatile system that enables reversible confinement of cells in a standard 12-well plate. Micropatterned devices were designed to establish a consistent cell confinement height in a vast array, segmented by feed channels for more uniform distribution of fresh nutrients to the culture. After experiments, the system can be disassembled, and the cells can be fixed, stained, and mounted to glass slides for long-term storage. This enables visualization and image analysis of large populations of dividing cells through confocal imaging, which shows the geometry and distribution of intracellular components during confinement.

2.1 PDMS micropattern

The PDMS substrate for compressing cells was fabricated using standard soft lithography. The master mold was created using KMPR 1000 series [Microchem] negative photoresist. KMPR 1005 was spun at 2,000 rpm for the first layer, corresponding to the 7 μm post confinement height. The subsequent 50 μm bypass channel layer was spun using KMPR 1050 at 2,500 rpm.

2.2 Microfluidic insert

The full structure for a single well-plate insert consists of two poly-dimethylsiloxane (PDMS) components, and is illustrated in Fig. 2a. The bottom piece contains the micropattern, and was cured at a base:crosslinker ratio of 10:1 (~1 MPa) with a height of 1.5 mm and an inlet for media flow of 0.35 mm in diameter. The softer top component was cured at a 40:1 ratio to a height of 3 mm, with an 8 mm inlet. This soft piece serves as a gasket between the micropattern piece and the top compression plate. Both of these pieces were punched using a 17 mm core borer, and were permanently bonded together with air plasma [Harrick] in a configuration that left the micropattern on the external face to compress cells.

When the micropattern (Fig. 2b) is securely placed over the cells, media is flown through a single inlet in the center, which distributes fresh media to each confinement region via the bypass channels, and prevents drying. Posts are positioned within the confinement regions to prevent channel collapse. The array of confinement regions are designed to maximize the number of confined cells, while enabling the presence of the bypass channels of significantly larger height (50 μm) which also house the control group of unconfined cells. The 50 μm height of the bypass channels results in significantly lower fluidic resistance compared to the 7 μm height of the confinement region, thereby facilitating sufficient solution exchange throughout the device.

2.3 Confinement system

For a 12-well plate, we machined a confinement lid by inserting 12 screw-in polycarbonate reservoirs into a flat poly-methyl methacrylate (PMMA) piece. These reservoirs can each hold a maximum of 1.5 mL of media to gradually transfer to the confined cells. The outer threading of the reservoir pieces allow adjustment of their heights in relation to the bottom of the well, if necessary. Twelve PDMS devices were autoclaved, and subsequently UV sterilized along with a vacuum chamber and the confinement plate. Each device was placed on the bottom of these reservoirs, taking advantage of the high adhesive strength of the gasket pieces. All parts of the system were placed in a sterile vacuum chamber to maintain sterility before confinement. Additionally, keeping the PDMS devices under vacuum minimized bubbles during confinement, and allowed better adhesion of the devices with the cover glasses at the bottom of the wells.

2.4 Cell culture

Prior to seeding, all coverslips were acid-cleaned, UV sterilized, plasma cleaned, and coated with 10 μg/mL of human plasma fibronectin. Three cell types from ATCC, HeLa cervical cancer, A375 melanoma, and A549 lung cancer were used in these studies. Upon reaching confluency, cells were passaged using conventional techniques and were reconstituted in the same volume of media. Roughly 5 % of these cells were seeded onto the coverslips, which were placed in a 12-well plate for at least 2 h to ensure uniform and confluent cell seeding. The cells were then subject to a double-thymidine block (Sánchez et al. 1993) to synchronize the cells at the interface of G1 and S phase, thereby facilitating the

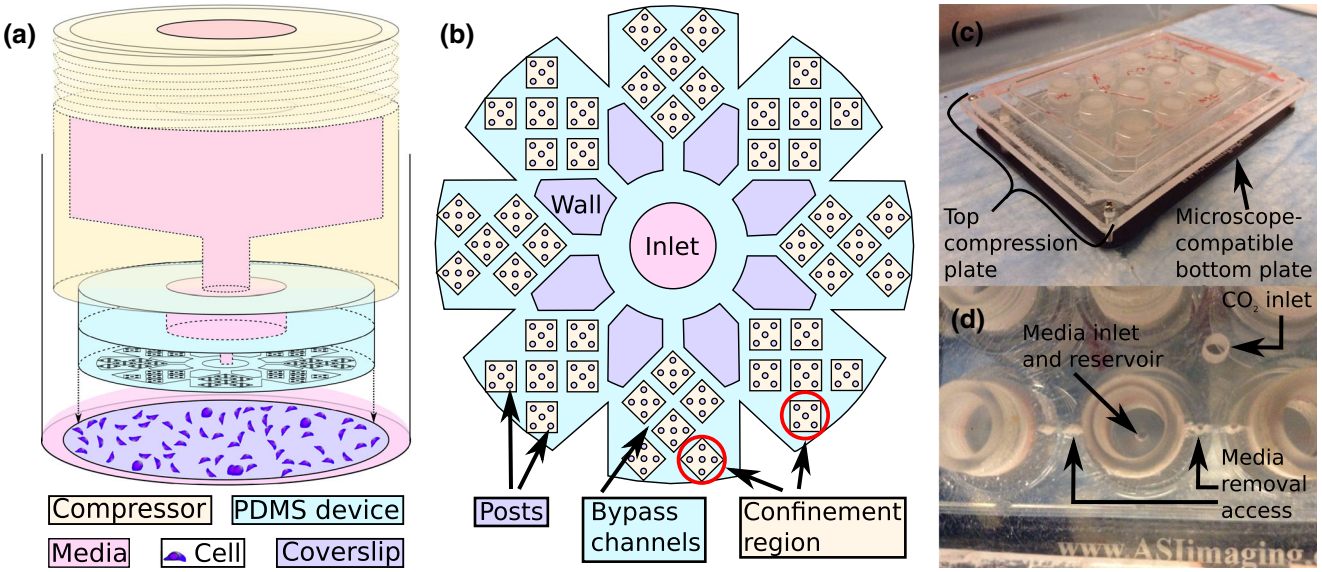

Fig. 2 Schematic of the confinement insert. **a** The PDMS insert is adhered to the bottom of the screw-in well via the soft gasket layer, and is pressed evenly onto coverslips with a confluent cell culture. **b** Bottom-up view displays a micropattern that is placed on top of the cell culture. Solution flows from the central inlet via the bypass channels to evenly distribute into the array of confinement squares. **c** Full view and **d** zoomed-in view provide images of the compression plate and its features for maintaining optimum CO_2 and fresh media

observation of mitotic cells. We observed significantly higher rates of cell death and asymmetric divisions, along with a significant reduction in multipolar divisions in HeLa cells that were untreated (Online Resource 1). This suggests that delays in S phase resulted in supernumerary centrosomes, which increased the likelihood of more than 2 progeny. For consistency and as a proof-of-concept of the technology, we applied the double-thymidine block for all experiments.

Upon release of this block, cells were confined. Cell density was quantified by the average cell matter coverage of the available confinement area. In A375 cells, we found that cell density >50 % prevented cell flattening, and density <10 % resulted in >90 % cell death (data not shown), so for long-term confinement studies the cell densities for all lines were kept between 20 and 50 %.

2.5 Confinement protocol

The 12-well plate containing the cell culture was secured into the microscope-compatible well-plate holder, as the compression plate was removed from vacuum. After ensuring that the inserts were securely fastened to the compression plate, the plate was lowered gently into the well plate as one piece, and the corners were screwed into the well-plate holder to maintain consistent compression over the course of the live-cell imaging experiments. The full protocol is detailed in Fig. 3.

2.6 Live imaging

To observe aberrant divisions occurring under confinement, the confinement platform was transferred to a fluorescence microscope [Nikon] with an incubated chamber set to 37 °C and 5 % CO_2. Multiple confinement regions were imaged every 10 min for 1–2 days, which was sufficient for obtaining a significant sample size of dividing cells. After the allotted time, 200 μL of 2 μM calcein AM and 4 μM ethidium homodimer was flowed through each inlet to ensure sufficient viability and as quality control to ensure that correct confinement was achieved. A lack of uniform confinement could be confirmed by dye staining outside of the confined or bypass channel.

2.7 Data analysis

A sample of ≥140 cells were categorized for both the confined and unconfined cases. For each cell type, an approximate peak for cell divisions was determined within the duration of live imaging (data not shown), and was used as the optimum time for cell fixation and staining.

2.8 Immunocytochemistry

Cells were incubated under confinement at 37 °C and 5 % CO_2. To increase the sample size of dividing cells to be visualized, the peaks times of cell division, determined from live imaging, were used as the duration of confinement in these experiments. At these peak times, 200 μL of fixation solution (4 % formaldehyde, 1 μg/mL Hoechst, 10 mM EDTA, 5 mM $MgCl_2$) was flowed through each inlet for 20 min to cross-link the cells and to simultaneously stain the nuclei. A nuclear stain (Hoechst 33342) was used to determine any leak into the walls of the channels, such that if the nuclei

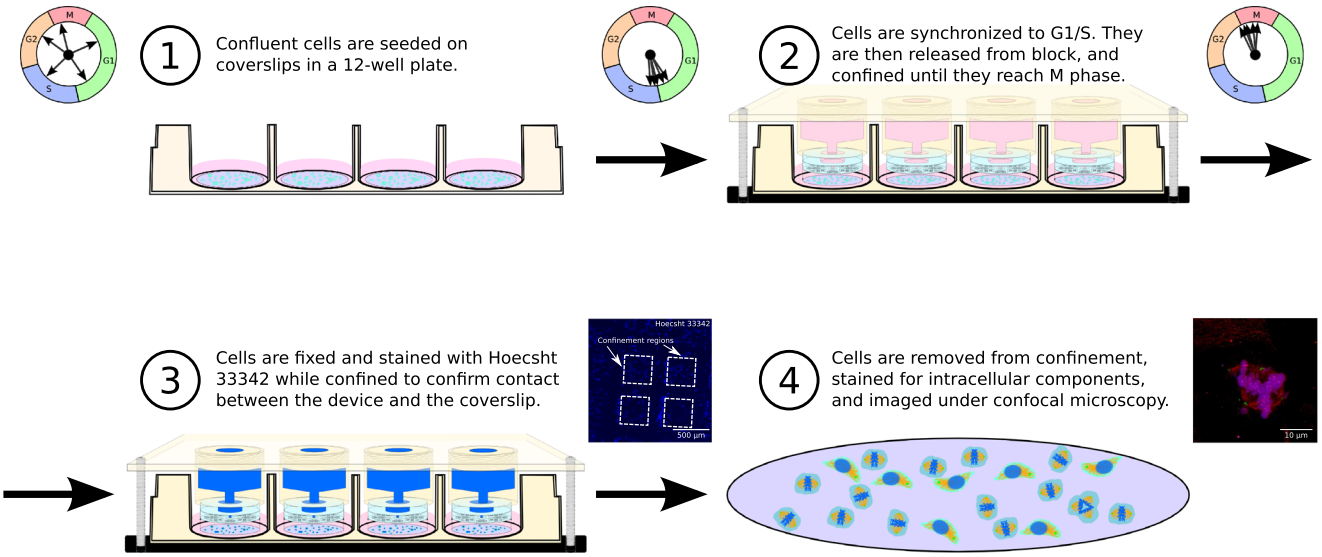

Fig. 3 Experimental protocol for confining cells, and staining to maximize the visualization of mitotic events due to confinement

of cells did stain in the walls, then the inserts were deemed as improperly confined, and were excluded from further staining and analysis.

Cells were permeablized with 0.2 % Triton X-100 for 20 min. After three PBS washes, coverslips were transferred to a petri dish [150 mm×15 mm] on top of a paraffin sheet on top of a moist paper towel. This was done to reduce the volume of reagents required to perform ICC, and to prevent drying. Coverslips were treated with blocking solution (5 % goat serum, 1 % BSA, and 0.1 % v/v Tween 20), followed by primary antibody incubation (blocking solution with 1:500 rabbit antipericentrin (Abcam, ab84542, lot GR30515), 1:250 chicken anti-alpha-tubulin (Abcam, ab89984, lot GR82981), 1:100 human anti-CREST (Antibodies Inc. 15-234-0001, lot 1CK32)) and secondary antibody incubation (blocking solution with 1:500 goat anti-rabbit, 1:250 goat anti-chicken, and 1:100 goat anti-human). Each incubation was done for 1 h at room temperature, with 3 blocking solution washes in between.

3 Results

3.1 Increased mitotic aberrations with confinement are cell line-dependent

Frequency and type of confinement-induced mitotic aberrations were cell line-dependent. Live cell brightfield time-lapse images enabled label-free quantification of aberrant divisions under confinement, as detailed in Fig. 4. At the normal end of the spectrum, A375 melanoma cells displayed the lowest frequency of aberrations, including multipolar divisions, asymmetric divisions, and fusions, though confined cells did have a significantly higher rate of such aberrations than unconfined cells. Yet, >45 % of cells underwent cell death in both the confined and unconfined case (Fig. 4a). This may be because extreme delays in mitosis and improper chromosome segregation under confinement triggered intact mitotic checkpoints to initiate cell destruction, which may signal unconfined cells as well. In order of significantly increasing abnormalities, 9.8 %, 14.2 %, and 32.5 % of confined A375, A549, and HeLa cells, respectively, produced asymmetric daughters (Fig. 4b, defined as divisions with >30 % difference in size between any two daughters). Furthermore, while 5.7 % of A375 cells produced three daughters (Online Resource 2), A549 and HeLa cells had an incidence of multi-polar divisions of 15.0 % and 24.6 %, respectively (Fig. 4d) (Online Resource 3). A549 cells produced as many as four progeny, while HeLas produced as many as five (Online Resource 4). Correspondingly, HeLa cells had the lowest rate of cell death upon confinement, suggesting that these cells maintained the highest stability under these conditions. Interestingly, a statistically significant proportion of A549 cells fused upon division compared to the other lines (Fig. 4c), though for all cells this occurrence was rare (<11 %).

3.2 Confinement leads to splayed metaphase plates and chromosome mis-segregation

Confocal imaging of chromosomes, MTs, centrosomes, and centromeres revealed significant chromosomal spreading with conserved patterns defined by centrosome positioning and MT length (Fig. 5). Confined A375 cells in general possessed the least aberrant phenotypes as observed by immunofluorescence, matching the results from live cell imaging Fig. 4. A375 cells form metaphase plates, but can fail to align some chromosomes, which were completely excluded from the spindle apparatus, but secured by polar astral MTs (Fig. 5a).

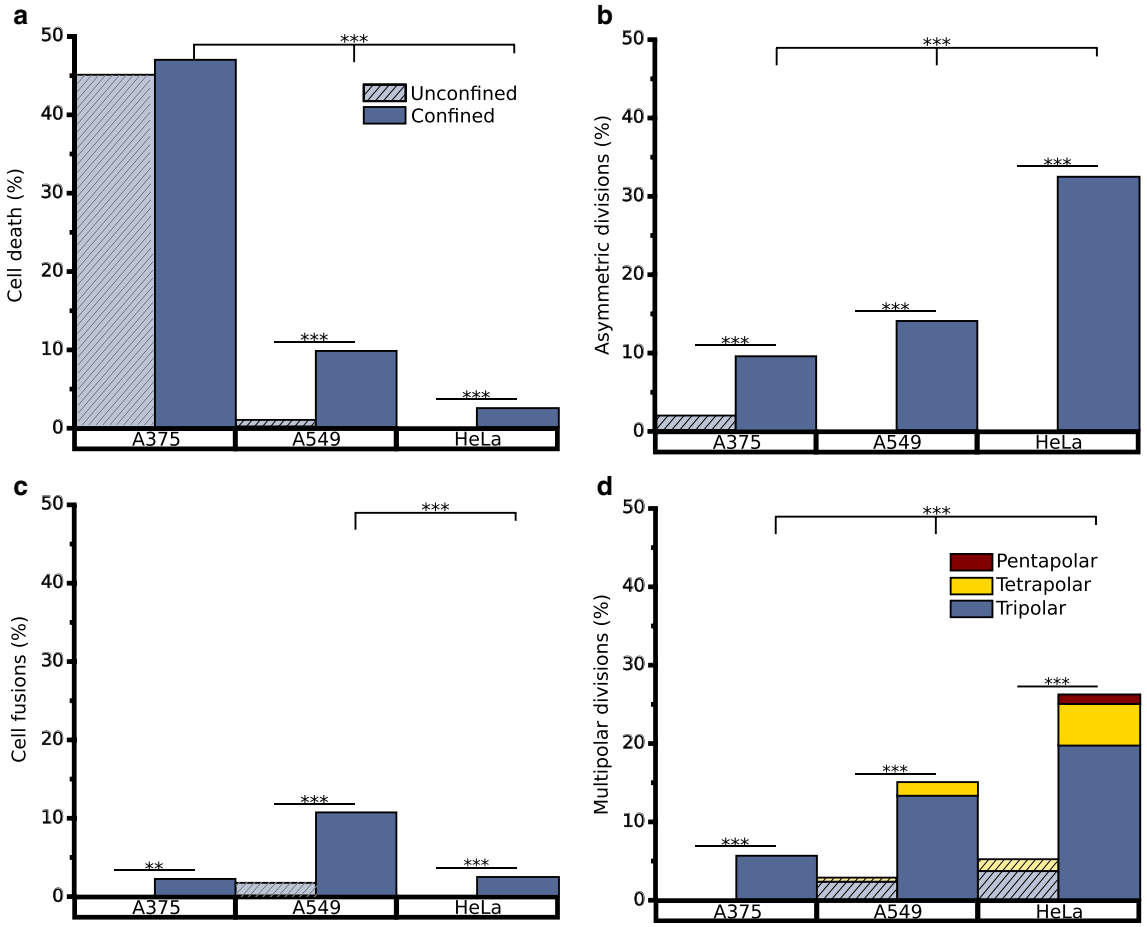

Fig. 4 Occurrence of anomalies under confinement. Populations of confined A375, A549, and HeLa cells were compared to unconfined cells for incidence of **a** cell death, **b** asymmetric divisions, **c** cell fusions, and **d** multipolar divisions (** = $p<0.05$ and *** = $p<0.01$)

In more common cases, the chromosomes are within the reach of the dynamic MTs, but may align parallel to them (Fig. 5b). We identified more pronounced segregation anomalies in A549 cells, where many confined cells showed a large splaying of DNA such that the metaphase plate formed in the plane of confinement. Figure 5c contains many cells in late anaphase or telophase, where the chromosomes have segregated, but this may suggest a positioning of the centrosomes to ideal locations. This is further evidenced by Fig. 5d, which shows a high magnification asymmetric tri-daughter A549 division. Higher order multipolar cytokinesis events were commonly observed in confined HeLa cells, including tetradaughter divisions (Fig. 5e) and rare pentadaughter divisions (Fig. 5f). In both cases, we see radially symmetric MT extensions with relatively uniform lengths emerging from the centrosomes. Chromosome locations appear to correspond with the limits of radial extension of MTs and display similar symmetry. The centrosomes in these multi-daughter divisions appear less punctate (Fig. 5e, f), which may be due to clustering of several centrosomes. In the case of the penta-daughter division (Fig. 5f) centrosomes occupy five optimal positions that permit equidistant extension of MTs to the kinetochores. Cells with supernumerary centrosomes can assume a variety of configurations for spindle stabilization (Fig. 5g, h). For example, in Fig. 5h the pentapolar spindle consists of a central cluster of centrosomes that complements four other equidistant pole. HeLa cells are not limited to pentapolar spindles; we do report the observation of a higher-order configuration (Online Resource 5), but at that stage, it becomes difficult to accurately visualize the exact number of poles.

Because the increased hydrostatic pressure of mitotic cells is insufficient to displace the stiff substrate, the acto-myosin cortex is forced to take on an irregular configuration. We next evaluated whether confined cells extended microtubules over longer distances to compensate for their elongated shapes during mitosis. To do this, we characterized the degree of flattening of confined and unconfined HeLa cells (Fig. 6a), as well as the maximal distance between centrosomes and centromeres (Fig. 6b). Confined cells show a 87.4 % increase in cell area, and a 13.3 % increase in centrosome-centromere distance, confirming that the cells are being significantly flattened although modification of position of the centrosomes

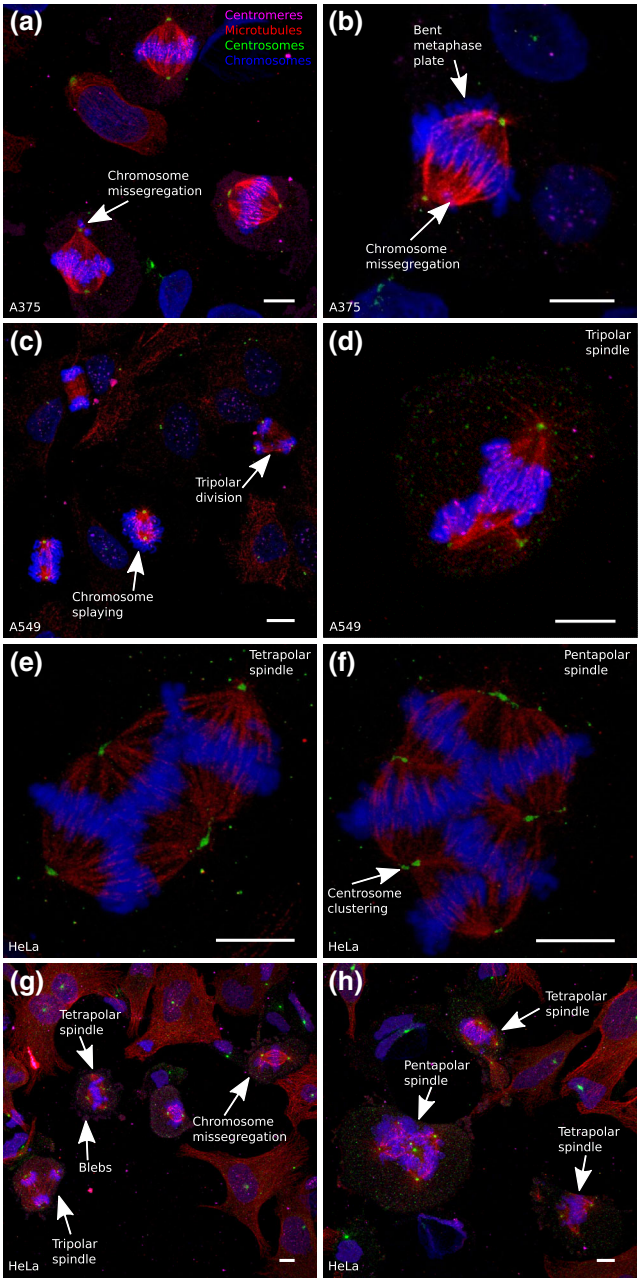

Fig. 5 Immunofluorescence stains of confined cells reveal a variety of mitotic aberrations. **a**–**b** show A375 cells that form metaphase plates, but failed to align all chromosomes. **b** shows a more pronounced form where much of the DNA has oriented abnormally in a plane that is co-planar with the MTs. **c**–**d** shows A549 cells undergoing chromosomal splaying and tridaughter divisions. **c** identifies a cell that is attempting to segregate chromosomes that are closer to its astral microtubules. The other cells appear to be in late anaphase or telophase, where the DNA is beginning to reach the centrosomes. **d** reveals a tridaughter division where the attachment of the microtubules to the kinetochores implies asymmetric arrangement of the chromosomes. **e**–**f** are singular images of the most extreme cases of flat mitosis in HeLa cells, where cells are undergoing (**e**) tetrapolar and (**f**) pentapolar divisions. **g**–**h** show the full range of aberrant multi-daughter asymmetric divisions, chromosome missegregation, and plasma membrane blebbing in HeLa cells. Scalebar = 10 μm

is minor. Though not very statistically significant ($p<0.1$), the additional distance that the MT must extend in confined cells may be enough to account for the chromosome missegregation that we observe. Several works suggest strong positive correlation between MT length and cytoplasmic volume (Good et al. 2013; Hazel et al. 2013; Wühr et al. 2008). However, it is important to note that in our studies, cell area is increased with a conservation in cytoplasmic volume, which aligns with experimental conditions and subsequent observations by Lancaster et al. (2013).

Average chromosome area in the XY plane increased by 38.5 % (Fig. 6c), while average circularity decreased by 37.3 % (Fig. 6d) in confined cells. These results were also only significant at $p<0.1$ level, which was expected as chromosome density still remains constant and z-height reduction is assumed to be uniform.

$$C = \frac{4\pi A}{p^2} \tag{1}$$

where

C is circularity
A is area, and
p is perimeter.

4 Discussion

The variation of aberration frequency across cell lines may result from a vast number of genomic differences among them. Spectral karyotyping of HeLa and A549 reveal drastic differences in individual chromosome number and translocations (Luk et al. 2001; Macville et al. 1999). Pre-existing mutations in the SAC will facilitate the initiation of anaphase despite chaotic conditions. Average centrosome number of the population will influence the rate of onset of multipolar configurations. A549 cells have been documented as having multiple centrosomes in 46 % of its population (Jiang et al. 2005). Furthermore, for multipolar divisions, copy number for each chromosome will influence the viability of daughter cells. For example, while HeLa is considered to be a hypertriploid line (3n+), A549 and A375 are hypotriploid (3n-) [ATCC], which may partially explain why HeLa cells were more likely to generate viable multidaughter progeny. Although the HeLa cell line has been sequenced, A549 has not, and further detailed genomic sequencing data would be required to elucidate molecular mechanisms responsible for the different behaviors between cell lines under confinement.

Another key result is the fairly consistent length of microtubules, independent of cell diameter during division. The conserved microtubule lengths, even for higher order multipolar divisions, appears to be enabled by coordinated positioning

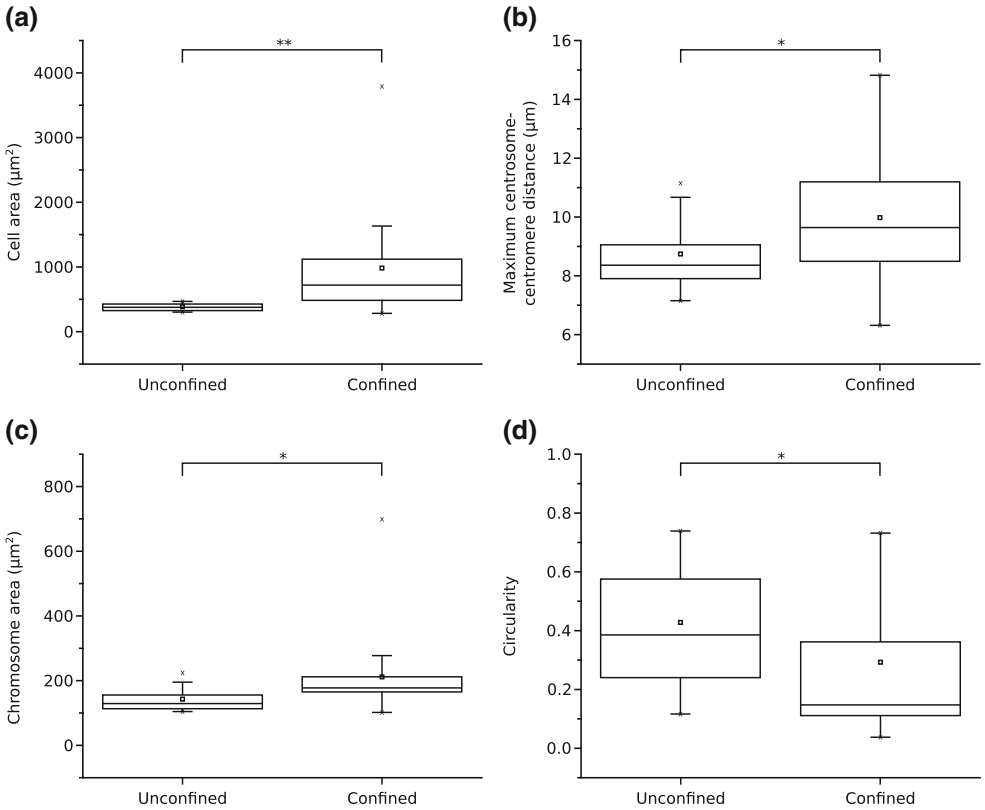

Fig. 6 Confined and unconfined HeLa cells are compared in the XY plane in terms of **a** cytosolic area, **b** maximum centrosome-centromere distance, **c** chromosome area, and **d** circularity. Confined cells display significant increases in cytosolic area, and slight increases in DNA area and centrosome-centromere distance, as well as a slight decrease in circularity (* = $p<0.10$ and ** = $p<0.05$)

of the centrosomes. Previous works seem to agree that in the presence of supernumerary centrosomes, the dividing cell spends a majority of mitosis in a stable multipolar configuration (Ganem et al. 2009; Krämer et al. 2011), most likely due to the establishment of sufficient tension of the kinetochore-attached MTs, which widens the spatial separation of aurora B kinase from its kinetochore substrates (Liu et al. 2009). This causes a reduction in phosphorylation of kinetochore substrates, and fulfills the SAC checkpoint of stabilized microtubule-kinetochore attachment (Liu et al. 2009). As part of this stabilization, non-kinetochore microtubules (those that extend to the midzone without binding to kinetochores) then contribute polar ejection forces (Antonio et al. 2000; Rieder and Salmon 1994) to chromosome arms, which orient the chromosomes at the metaphase plate. However, in response to multipolar configurations, it is clear that unusual metaphase plates are produced (Fig. 5e–f).

To produce viable progeny, these multipolar configurations and unusual metaphase plates must then form abnormal cleavage furrows (Wheatley and Wang 1996) during subsequent cytokinesis. Though cleavage onset is beyond the scope of this study, we report unusual observations for daughter cell separation under confinement. As opposed to the normally circular, symmetric divisions, confined cell daughters tend to separate abruptly, sometimes ejecting bleb-like structures. Even in confined cells that underwent bipolar symmetric divisions, cleavage was misshapen. Several models of cleavage furrow placement have been proposed, yet there is currently no prevalent theory on the exact underlying mechanisms (Burgess and Chang 2005). Though our findings do not directly support any model over another, our confinement system may be used as a rapid method for inducing unusual cleavage furrows. Induction of offset metaphase plates (as seen in bipolar asymmetric divisions) or unusual metaphase plate geometries (as seen in multipolar divisions) in high throughput may assist in developing a better understanding of the level of contribution of different types of MTs to cleavage formation (Alsop and Zhang 2003; Burgess and Chang 2005).

Though multi-polar mitotic events were rare in A375 cells, we were surprised to find that the frequency was greatly increased with a reduction in confinement height. Cells that remained viable after being subjected to near-zero height were significantly more likely to undergo higher order multidaughter divisions (Online Resource 6). The presence of multiple centrosomes in such levels of confinement were absent from confinement at 7 μm, which may suggest that centrosome amplification is a cellular response to limited space and subsequent splaying of chromosomes. Borel, et al. give evidence to support the idea that supernumerary centrosomes arise from an override of the tetraploidy checkpoint and failure to arrest in G1 (2002), which may potentially be induced by abnormal spindle formation from increasing levels

of confinement, followed by progression into the next cell cycle. Interestingly, Hut, et al. report that when DNA is improperly replicated or is damaged, there is an increased likelihood of centrosome splitting into multiple structures that contain single centrioles (2003). The level of confinement in these A375 cells is sufficient to induce lamina rupture (Le Berre et al. 2012), which may trigger centrosome splitting and multipolar cytokinesis. However, a true understanding of the mechanisms behind this phenomenon will require further studies of these cells under several well-controlled heights. Though our previous confinement approach explored the impact of lower confinement heights on HeLa cells (Tse et al. 2012), our current device can ensure a more uniform height with higher N that can be compatible with long-term fluorescent live-cell imaging to facilitate tracking of centrosome duplication or splitting.

5 Conclusion

We have developed a platform that permits long-term studies of physical disruption of spindle assembly and chromosome segregation on a large number of cells in parallel. It offers the unique advantages of simplicity of use with standard cell culture and well-plate formats, as well as uniform distribution of any media or solution to be used in tandem with confinement experiments. We have shown that cells of varying genetic makeup, origin, and morphology differ in response to confined conditions. This technology may serve as a reliable method for cell biologists to study more specific genetic pathways involved in mitosis and response to confinement.

Acknowledgments The authors would like to thank Yeganeh Amini, Coleman Murray, Dr. Matthew Schibler, and Nikhil Kalluri for their assistance in this work. Confocal laser scanning microscopy was performed at the CNSI Advanced Light Microscopy/Spectroscopy Shared Resource Facility at UCLA, supported with funding from NIH-NCRR shared resources grant (CJX1-443835-WS-29646) and NSF Major Research Instrumentation grant (CHE-0722519).

Ethics statement The manuscript does not contain clinical studies or patient data. The authors declare that they have no conflict of interest.

References

G.B. Alsop, D. Zhang, J. Cell Biol. **162**, 383 (2003)
C. Antonio, I. Ferby, H. Wilhelm, M. Jones, E. Karsenti, A.R. Nebreda, I. Vernos, Cell **102**, 425 (2000)
F. Borel, O.D. Lohez, F.B. Lacroix, R.L. Margolis, Proc. Natl. Acad. Sci. U. S. A. **99**, 9819 (2002)
D.R. Burgess, F. Chang, Trends Cell Biol. **15**, 156 (2005)
K.F. DeLuca, S.M.A. Lens, J.G. DeLuca, J. Cell Sci. **124**, 622 (2011)
C. Ditchfield, V.L. Johnson, A. Tighe, R. Ellston, C. Haworth, T. Johnson, A. Mortlock, N. Keen, S.S. Taylor, J. Cell Biol. **161**, 267 (2003)
N.J. Ganem, S.A. Godinho, D. Pellman, Nature **460**, 278 (2009)
M.C. Good, M.D. Vahey, A. Skandarajah, D.A. Fletcher, R. Heald, Science **342**, 856 (2013)
D.J. Gordon, B. Resio, D. Pellman, Nat. Rev. Genet. **13**, 189 (2012)
J. Hazel, K. Krutkramelis, P. Mooney, M. Tomschik, K. Gerow, J. Oakey, J.C. Gatlin, Science **342**, 853 (2013)
M. Hetzer, O.J. Gruss, I.W. Mattaj, Nat. Cell Biol. **4**, E177 (2002)
H.M.J. Hut, W. Lemstra, E.H. Blaauw, G.W.A. Van Cappellen, H.H. Kampinga, O.C.M. Sibon, Mol. Biol. Cell **14**, 1993 (2003)
T. Itabashi, Y. Terada, K. Kuwana, T. Kan, I. Shimoyama, Proc. Natl. Acad. Sci. U. S. A. **109**, 7320 (2012)
F. Jiang, N.P. Caraway, R. Li, R.L. Katz, Oncogene **24**, 3409 (2005)
A. Krämer, B. Maier, J. Bartek, Mol. Oncol. **5**, 324 (2011)
O.M. Lancaster, M. Le Berre, A. Dimitracopoulos, D. Bonazzi, E. Zlotek-Zlotkiewicz, R. Picone, T. Duke, M. Piel, B. Baum, Dev. Cell **25**, 270 (2013)
M. Le Berre, J. Aubertin, M. Piel, Integr. Biol. **4**, 1406 (2012)
C.L. Limoli, M.I. Kaplan, E. Giedzinski, W.F. Morgan, Free Radic. Biol. Med. **31**, 10 (2001)
W.L. Lingle, S.L. Barrett, V.C. Negron, A.B. D'Assoro, K. Boeneman, W. Liu, C.M. Whitehead, C. Reynolds, J.L. Salisbury, Proc. Natl. Acad. Sci. U. S. A. **99**, 1978 (2002)
D. Liu, G. Vader, M.J.M. Vromans, M.A. Lampson, S.M.A. Lens, Science **323**, 1350 (2009)
X. Lu, Y. Kang, Cancer Res. **69**, 8536 (2009)
C. Luk, M.S. Tsao, J. Bayani, F. Shepherd, J.A. Squire, Cancer Genet. Cytogenet. **125**, 87 (2001)
M. Macville, E. Schröck, H. Padilla-Nash, C. Keck, B.M. Ghadimi, D. Zimonjic, N. Popescu, T. Ried, Cancer Res. **59**, 141 (1999)
L. Menendez, B.B. Benigno, J.F. Mcdonald, Mol. Cancer **3**, 1 (2004)
M. Nishigaki, K. Aoyagi, I. Danjoh, Cancer Res. **65**, 2115 (2005)
G.A. Pihan, J. Wallace, Y. Zhou, P. Carcinomas, Cancer Res. **63**, 1398 (2003)
C.L. Rieder, E.D. Salmon, J. Cell Biol. **124**, 223 (1994)
I. Sánchez, L. Goya, A.K. Vallerga, G.L. Firestone, Cell Growth Differ. **4**, 215 (1993)
M.P. Stewart, J. Helenius, Y. Toyoda, S.P. Ramanathan, D.J. Muller, A.A. Hyman, Nature **469**, 226 (2011)
M. Théry, V. Racine, A. Pépin, M. Piel, Y. Chen, J.-B. Sibarita, M. Bornens, Nat. Cell Biol. **7**, 947 (2005)
H.T.K. Tse, W.M. Weaver, D. Di Carlo, PLoS One **7**, e38986 (2012)
P. Tseng, J.W. Judy, D. Di Carlo, Nat. Methods **9**, 1113 (2012)
S.P. Wheatley, Y. Wang, J. Cell Biol. **135**, 981 (1996)
A.S. Wilson, B.E. Power, P.L. Molloy, Biochim. Biophys. Acta **1775**, 138 (2007)
M. Wühr, Y. Chen, S. Dumont, A.C. Groen, D.J. Needleman, A. Salic, T.J. Mitchison, Curr. Biol. **18**, 1256 (2008)
S. Yasuda, T. Oceguera-Yanez, F. Kato, M. Okamoto, Y. Yonemura, S. Terada, T. Ishizaki, N. Shuh, Nature **428**, 767 (2004)